

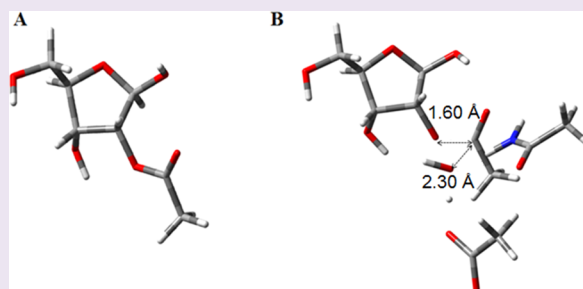
# Transition-State Analysis of 2-O-Acetyl-ADP-Ribose Hydrolysis by Human Macrodomain 1

Brett M. Hirsch, Emmanuel S. Burgos, and Vern L. Schramm\*

Department of Biochemistry, Albert Einstein College of Medicine, 1300 Morris Park Avenue, Bronx, New York 10461, United States

## Supporting Information

**ABSTRACT:** Macrodomains, including the human macrodomain 1 (MacroD1), are erasers of the post-translational modification of monoadenosinediphospho-ribose and hydrolytically deacetylate the sirtuin product *O*-acetyl-ADP-ribose (OAADPr). OAADPr has been reported to play a role in cell signaling based on oocyte microinjection studies, and macrodomains affect an array of cell processes including transcription and response to DNA damage. Here, we investigate human MacroD1 by transition-state (TS) analysis based on kinetic isotope effects (KIEs) from isotopically labeled OAADPr substrates. Competitive radiolabeled-isotope effects and mass spectrometry were used to obtain KIE data to yield intrinsic KIE values. Intrinsic KIEs were matched to a quantum chemical structure of the TS that includes the active site residues Asp<sup>184</sup> and Asn<sup>174</sup> and a structural water molecule. Transition-state analysis supports a concerted mechanism with an early TS involving simultaneous nucleophilic water attack and leaving group bond cleavage where the breaking C–O ester bond = 1.60 Å and the C–O bond to the attacking water nucleophile = 2.30 Å. The MacroD1 TS provides mechanistic understanding of the OAADPr esterase chemistry.



Macrodomains are an evolutionarily conserved family of enzymes and protein domains that recognize NAD<sup>+</sup>-derived metabolites. These include mono- and poly-ADP-ribose (ADPr), ADP-ribosylated proteins, and the product of sirtuin deacetylase reactions, 2-*O*-acetyl-ADP-ribose (OAADPr).<sup>1–6</sup> ADP-ribosylation is a reversible protein post-translational modification impacting cellular processes including transcription, neuronal signaling, and response to stresses such as infection and DNA damage.<sup>7–13</sup> ADP-ribosyltransferases also influence biological pathways through poly- and mono-ADPr polymerases including diphtheria toxin-like ADP-ribosyltransferases and the clostridial toxin-like ADP-ribosyltransferases.<sup>9,10,14–17</sup> Macro D1 and other macrodomain family members including human MacroD2, C6orf130, and archaeal Af1521 have esterase activity toward the acetyl group of OAADPr and hydrolytic activity for mono-ADP-ribosylated proteins.<sup>18</sup>

Macrodomains related to MacroD1 bind OAADPr and hydrolyze the 2-ester bond to generate ADPr and acetate as products.<sup>18–22</sup> The OAADPr product of sirtuin NAD<sup>+</sup>-dependent deacetylases has been implicated as a signaling molecule. Thus, macrodomains may function in the regulation of cellular OAADPr levels and downstream signaling in the sirtuin pathways (Figure 1).<sup>23</sup> A functional link is also suggested by reports that macrodomains are physically or genetically linked to histone deacetylases.<sup>23–25</sup>

We investigated the TS structure of human MacroD1 in its esterase activity toward OAADPr. Isotopically labeled OAADPr molecules were synthesized and used in kinetic isotope effect (KIE) studies.<sup>5</sup> Macrodomains related to MacroD1 have been

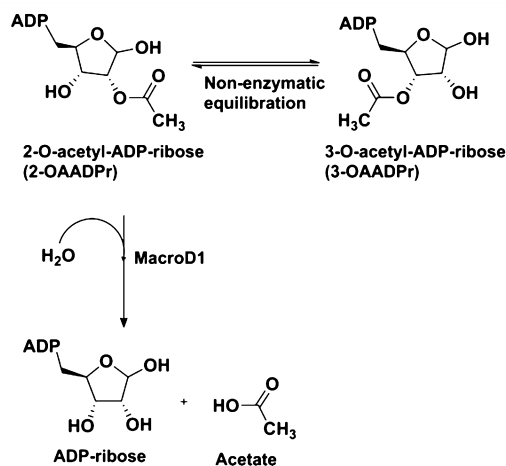


**Figure 1.** MacroD1 catalyzes the hydrolysis of the sirtuin product *O*-acetyl-ADP-ribose by hydrolysis of the 2-*O*-ester bond to form ADP-ribose and acetate.

discovered in all kingdoms of life including yeast (enzyme POA1p) and *Archaeoglobus fulgidus* (enzyme Af1521). MacroD1 is one of 11 annotated human macrodomains whose founding member is histone protein macroH2A1.1.<sup>21,26</sup> MacroD1 overexpression has been linked to the progression of

Received: April 8, 2014

Accepted: July 22, 2014

Published: July 22, 2014

**Table 1. Steady-State Parameters of MacroD1<sup>a</sup>**

	pH 6.8	pH 7.3 <sup>b</sup>
$K_m$ ( $\mu\text{M}$ )	1400 $\pm$ 400	370 $\pm$ 50
$k_{\text{cat}}$ ( $\text{s}^{-1}$ )	0.72 $\pm$ 0.01	0.20 $\pm$ 0.04
$k_{\text{cat}}/K_m$ ( $\text{s}^{-1} \text{M}^{-1}$ )	(4.9 $\pm$ 0.28) $\times 10^2$	(5.3 $\pm$ 1.2) $\times 10^2$

<sup>a</sup>Values represent catalyzed hydrolysis of OAADPr at pH 6.8 and 7.3.

<sup>b</sup>Values taken from Chen et al.<sup>1</sup>

breast cancer, and a loss-of-function mutation of macrodomain C6orf130 is responsible for a lethal neurodegeneration.<sup>27–29</sup>

The classic mechanism of ester hydrolysis proceeds in two steps including a kinetically reversible tetrahedral intermediate. M.L. Bender in 1951 observed <sup>18</sup>O-exchange from the carbonyl of ethyl benzoate into solvent during the reaction, supporting a diol intermediate.<sup>30</sup> Our analysis of the TS for MacroD1 is different and supports a concerted mechanism. Thus, the TS of MacroD1 shows significant bond order to the attacking water nucleophile and significant bond loss for the acetate leaving group.

Kinetic isotope effects provide experimental guides to computational chemistry for the understanding of enzymatic TSs. Enzymatic TS analysis based on  $k_{\text{cat}}/K_m$  competitive KIEs provides a two state analysis. It compares the structure and geometry of free reactant to that of the TS and includes all steps between reactant and the first chemically irreversible step. At the TS, bond orders, angles, and molecular electrostatic potentials can be extracted from the wave function.<sup>31,32</sup> Transition state analysis does not provide information on steps after the TS, but these can often be deduced from likely paths to product from the detailed knowledge of the TS. Experimentally determined KIEs are paired with density function theory (DFT) to determine the TS structure of the enzymatic reaction, here applied to the deacetylation of OAADPr by MacroD1.

We used two independent methods of obtaining KIE data at mechanistically critical atomic positions. The combination of radio-isotope labeling and mass spectrometry in competitive assays confirmed the data obtained by both methods. The intrinsic isotope effects were used to generate an electrostatic potential surface (ESPS) map, a tool for understanding the electron distribution at the transition state. In other systems, this approach has provided a starting point for the design of TS analogues. This approach has been successful in inhibiting ribosyl transfer enzymes including purine nucleosidase phosphorylases. Transition state analogues of MacroD1 would be useful in exploring functions of OAADPr.<sup>33,34</sup> Here,

the structure of the MacroD1 TS provides chemical insight into the mechanism of MacroD1 ester hydrolysis.

## RESULTS AND DISCUSSION

**Purification and Activity of Protein.** Human Macrodomain 1 was produced from its cDNA, overexpressed in *E. coli* with an N-terminal 6xHis tag and purified to homogeneity based on SDS-PAGE analysis. The DNA sequence encoding MacroD1 was validated by nucleotide sequencing. The MacroD1 structure contains a macrodomain and an N-terminal region. The macrodomain portion is made of a distinct fold containing a six stranded  $\beta$ -sheet between two  $\alpha$ -helices.<sup>1</sup>

Steady-state parameters for OAADPr hydrolysis to ADPr and acetate were determined in reactions containing MacroD1, OAADPr, and pH 6.8 sodium phosphate at 25 °C (Table 1).

At pH 6.8, catalytic rates are near-optimal and base-catalyzed, nonenzymatic hydrolysis of the ester bond is minimized. Under these conditions, nonenzymatic hydrolysis was insignificant for at least 1 h (SI Figure S3).

Kinetic parameters determined under these conditions were similar to reported values, and the  $k_{\text{cat}}$  of the hydrolysis rates were equivalent at pH values from 6.5 to 8.0 (SI Figure S4). The specific rate constant for the nonenzymatic 3- to 2-transesterification reaction of the acetate moiety ( $k_{3\rightarrow 2}$ ) was determined as previously described.<sup>35</sup> Under these conditions, transesterification had a first-order rate constant of  $1.81 \times 10^{-2} \text{ s}^{-1}$ . Thus, 3-O-AADPr was found to nearly equilibrate after 3 min under these conditions (SI Figure S5).

**Commitment to Catalysis ( $C_f$  and  $C_r$ ).** Intrinsic KIEs are required to provide TS information. They are obtained from experimental KIEs by correction for the forward and reverse commitment to catalysis. Forward commitment ( $C_f$ ) is the probability for the substrate-enzyme complex to form products rather than return to free enzyme and substrate. Reverse commitment is the probability of the enzyme bound products to form substrate rather than dissociating from the enzyme. The forward commitment can be determined by isotope-trapping experiments pioneered by I. Rose.<sup>35</sup> Substrate trapping experiments with MacroD1 and labeled 2-O-AADPr, gave a  $C_f$  of less than 1% (SI Figure S6). Competitive KIEs measure all enzymatic steps from free OAADPr to the first kinetically irreversible step. For MacroD1, reverse commitment is expected to be negligible, as MacroD1, such as most hydrolases, is kinetically irreversible under our experimental conditions.

**Intrinsic KIEs.** The family of intrinsic KIE values associated with labeled 2-O-AADPr and MacroD1 show significant

**Table 2. Intrinsic and Calculated KIEs for the Hydrolysis of 2-O-AADPr Catalyzed by MacroD1<sup>a</sup>**

heavy isotope	light isotope <sup>b</sup>	KIE type	intrinsic KIE <sup>c</sup>	calculated KIE <sup>d</sup>
1- <sup>13</sup> C]-acetyl		primary	1.033 $\pm$ 0.006	1.034
1- <sup>14</sup> C]-acetyl	5-[ <sup>3</sup> H]-ribose	primary	1.059 $\pm$ 0.012	1.064
2- <sup>2</sup> H <sub>3</sub> ]-acetyl		$\beta$ -secondary	0.976 $\pm$ 0.003	0.976
2- <sup>3</sup> H <sub>3</sub> ]-acetyl	5-[ <sup>14</sup> C]-ribose	$\beta$ -secondary	0.971 $\pm$ 0.013	0.982
2- <sup>2</sup> H]-ribose		$\beta$ -secondary	1.062 $\pm$ 0.008	1.060
2- <sup>3</sup> H]-ribose	5-[ <sup>14</sup> C]-ribose	$\beta$ -secondary	1.169 $\pm$ 0.044	1.087
2- <sup>18</sup> O]-ribose		primary	1.039 $\pm$ 0.004	1.037

<sup>a</sup>Atomic position and value of all intrinsic KIEs with standard deviations compared to KIEs for the best fit transition state. <sup>b</sup>Light isotope refers to remote labels reporting on the reaction rate of the light isotopic reactant in competitive radio-isotope experiments. <sup>c</sup>Intrinsic KIE values have been corrected for commitments ( $C_f < 0.1\%$ ) and remote label KIE contributions. <sup>d</sup>The model for the TS included solution-phase (water) reactant states and an *in vacuo* TS. Calculated KIEs were determined from a reactant state model containing an average of the four variants known in the solution geometry for 2-endo and 3-endo ribose and  $\alpha$ - and  $\beta$ -anomers

intrinsic KIE values from both the acetyl and ribosyl groups (Table 2). For radioisotope-labeled OAADPr, intrinsic KIEs were obtained by measuring the observed KIE for the remote reporting labels 5- $^3\text{H}$  or 5- $^{14}\text{C}$  and correcting to give the intrinsic KIEs.

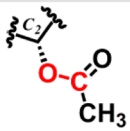
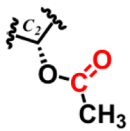
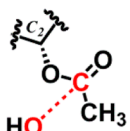
The relationships between  $^2\text{H}$  and  $^3\text{H}$  or  $^{13}\text{C}$  and  $^{14}\text{C}$  intrinsic KIEs are defined by the Swain–Schaad equations (eqs 1 and 2, respectively). The KIE values for MacroD1 agree with this relationship, with the exception at the tritiated 2-*H*-ribose position.<sup>36,37</sup>

$$\left(\frac{k_{\text{H}}}{k_{\text{T}}}\right) = \left(\frac{k_{\text{H}}}{k_{\text{D}}}\right)^{1.442} \quad (1)$$

$$r = \frac{\ln(k_{12}/k_{14})}{\ln(k_{12}/k_{13})} \quad \text{where } 1.8 \geq r \leq 2.0 \quad (2)$$

The primary 1- $^{13}\text{C}/^{14}\text{C}$ -acetyl KIEs, of 1.033 and 1.059, respectively, provide information on the TS by reporting on the hybridization change of the acetyl carbonyl carbon from  $\text{sp}^2$  toward  $\text{sp}^3$  as the nucleophile attacks.  $\text{Asp}^{184}$  has been proposed as the base for activation of the water nucleophile. The primary 2- $^{18}\text{O}$ -ribose KIE, 1.039, reports on the degree to which the ester bond order changes at the TS. Together, these KIE values support a mechanism of concerted nucleophile attack and ester bond cleavage rather than a stepwise reaction. This TS includes significant bond order to the approaching nucleophile and decreased bond order to the ribose-acetate ester bond (Table 3). In a step-wise mechanism, the ester bond order would be maintained through formation of a distinct tetrahedral intermediate.

**Table 3. Comparison of Bond Orders between the Reactant and Transition-States of Concerted MD1 Ester Hydrolysis (Ångstroms between Red Atoms)**

Bond	GS Bond Distance	TS Bond Distance	GS Bond Order	TS Bond Order
	1.43	1.60	1.00	0.753
	1.20	1.19	1.11	1.14
	—	2.30	—	0.264

$^{18}\text{O}$  KIEs have been studied under similar reactions for the nonenzymatic hydrolysis of *p*-nitrophenyl acetate (PNPA) in the presence of oxyanion nucleophiles. The reported KIE value was 1.028 at the phenolic (ester) oxygen. This KIE is smaller than the KIE found for MacroD1 and supports the concerted mechanism for MacroD1.<sup>38</sup>

The  $\beta$ -secondary 2- $^{2}\text{H}_3/^{3}\text{H}_3$ -methyl acetyl KIEs report on the rotational or out-of-plane freedom of these hydrogen atoms at the TS. The  $\beta$ -secondary KIE at the 2- $^{2}\text{H}/^{3}\text{H}$ -ribose position reports on the C2–H2 bond order due to electronic effects from the altered bond order to the O2 ester. All secondary  $^2\text{H}$  and  $^3\text{H}$  KIEs are subject to binding isotope effects from formation of the Michaelis complex, but the  $^{13}\text{C}$ ,  $^{14}\text{C}$ , and  $^{18}\text{O}$  are not.<sup>39</sup> Gaussian TS modeling correlates these values with changes in the ribose bond orders and geometry at the TS. Although the 2- $^{3}\text{H}$ -ribose value does not match the Swain–Schaad relationship or the computed value, the  $^2\text{H}$ -labeled ribose is an excellent match at this position.

**Modeling of the MacroD1 TS.** Calculations to match the intrinsic KIEs to a TS for MacroD1 TS used Gaussian 09<sup>40</sup> with the m062x/6-31g(d,p)<sup>41</sup> basis set. Atoms of the TS included a truncated OAADPr molecule (acetyl-ribose), one or two water molecules, and truncated mimics of the active site residues  $\text{Asp}^{184}$  and  $\text{Asn}^{174}$ . Transition state analysis by KIE analysis reports on the difference between the reactant state free in solution and the TS. Reactant state OAADPr was generated by optimizing the structure to locate the global energy minimum. The TS to match the intrinsic KIEs was found by iterating the bond lengths for both the forming and breaking C–O bonds as well as exploring conformations of the ribose ring pucker and anomeric conformations. All calculated TS structures were optimized to local energy minima. Theoretical KIE values were calculated for each optimized structure in ISOEFF98<sup>42</sup> for comparison to the intrinsic KIEs. The breaking and forming bond lengths and the distance between the ribose and aspartate mimic were the sole constraints imposed to generate the TS model. All other parameters were unconstrained. The TS that best matched the intrinsic KIEs was subject to additional analysis using polarizable continuum models (PCM) with dielectric constants of water or acetone as solvents. Atomic coordinate data for the reactant and transition-state optimizations can be found in the Supporting Information (Figure S7).

**Generating the Reactant State.** The two-state nature of TS analysis requires an accurate reactant state. The reactant state of OAADPr is complicated by the near-equal distributions of the 2-endo and 3-endo ribose puckers in both  $\alpha$ - and  $\beta$ -anomeric positions. Thus, four reactant state optimized geometries were used to generate four sets of KIE values for each transition-state. The average of the reactant states provided an unbiased representation of the actual reactant state structures and these calculated values were averaged to provide the final KIE values (Table 2). This process was needed to match the geometry-dependent  $\beta$ -secondary KIE values. However, primary KIE values were not significantly affected by ribose conformation in the reactant state.

Reactant state analysis also considered the effects of 2-*O* and 3-*O*-acetate chemical equilibrium. Transesterification equilibration on reactant states from 3-*O*-AADPr were evaluated through QM models and KIE calculations. The modeled KIE values from a 3-*O*-AADPr reactant state do not agree at the 2- $^{18}\text{O}$  ribose or 1- $^{13}\text{C}$  acetyl positions. The calculations establish that equilibration of the 3-OH to the reactive 2-*O*-AADPr species does not contribute significantly to the observed KIE values.

**Properties of the Transition State.** The computed TS structure provided a good match of calculated and intrinsic KIEs at four isotopically substituted positions (Table 2). The TS included significant bond order (*R*) to the attacking nucleophile ( $R_{\text{C-Nu}} = 0.264$ ) and departing acetate ( $R_{\text{C-O}} =$

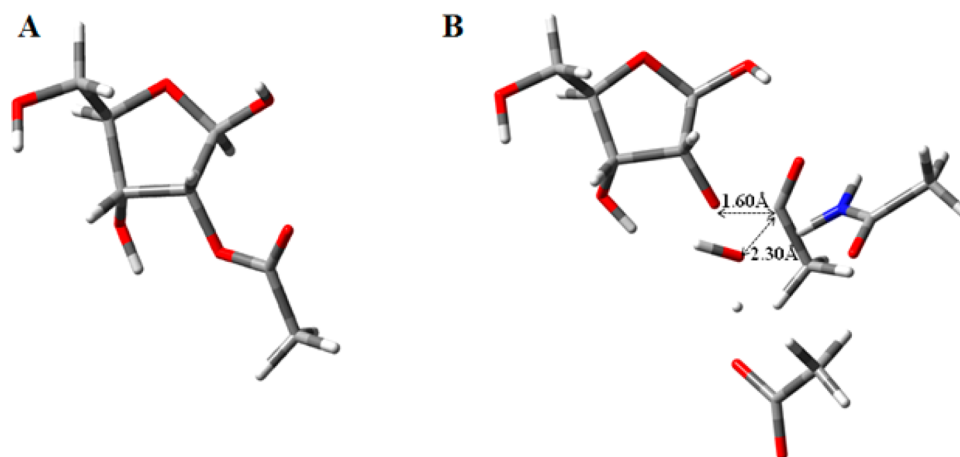


**Figure 2.** Ground and transition state structures. (A) Optimized reactant state of OAADPr in a water PCM model. (B) *In vacuo* modeled transition state based on m062x/6-31g(d,p) DFT calculations to best match the intrinsic KIE values. Carbon, hydrogen, oxygen, and nitrogen atoms, are represented in gray, white, red, and blue, respectively. Fragments of Asn<sup>174</sup> (below) and Asp<sup>184</sup> (right) were included in the QM computational region.

0.753) (Table 3; Figure 2; Scheme 1). This TS structure supports a concerted mechanism. The large KIE values and low forward commitment support this proposal. However, TS analysis provides no information beyond the first irreversible step; thus, the conversion of TS to products in Scheme 1A is a hypothetical, but logical, path from the TS. In a two-step reaction (Scheme 1B), water attack would form a tetrahedral intermediate before the ester bond to the ribosyl is broken. We find that the ribose-acetate bond is partially broken at the transition-state, off the path to intermediate formation (Scheme 1).

The best fit of the intrinsic 2-<sup>[2H/3H]</sup>-ribose KIE required a TS with a 2-endo ribose pucker, whereas the 3-endo TS did not match well at either secondary hydrogen KIE position. The 2-endo ribosyl geometry is similar to that in crystal structures obtained for ADPr in macrodomains with a active site residue homology to human MacroD1, also supporting the TS analysis.<sup>1</sup>

**Consideration of Stepwise TSs.** The mechanism for MacroD1 catalysis in a stepwise reaction with formation of a tetrahedral intermediate as the highest barrier (TS1, Scheme 1B) was eliminated. The calculated 2-<sup>[18O]</sup>-ribose KIEs for any chemically reasonable TSs for diol formation were 0.997–1.013, well outside the experimental error of the intrinsic KIE value of 1.039. Small 2-<sup>[18O]</sup>-ribose KIEs are a consequence of little change in bond order to the oxygen from reactant to intermediate.

The TS2 mechanism predicted KIE values for 1-<sup>[13C]</sup>-acetyl from 1.048 to 1.064 and 2-<sup>[18O]</sup>-ribose values from 1.054 to 1.057, well outside the experimental errors of intrinsic KIE values (1.034 and 1.039, respectively) for both positions (Table 2). The relatively large KIEs for TS2 result from large bond order changes to both ribosyl oxygen and acetyl carbon as the ester bond breaks at TS2. Thus, neither TS1 nor TS2 along a reaction coordinate to or from a diol intermediate agreed with the intrinsic KIE values.

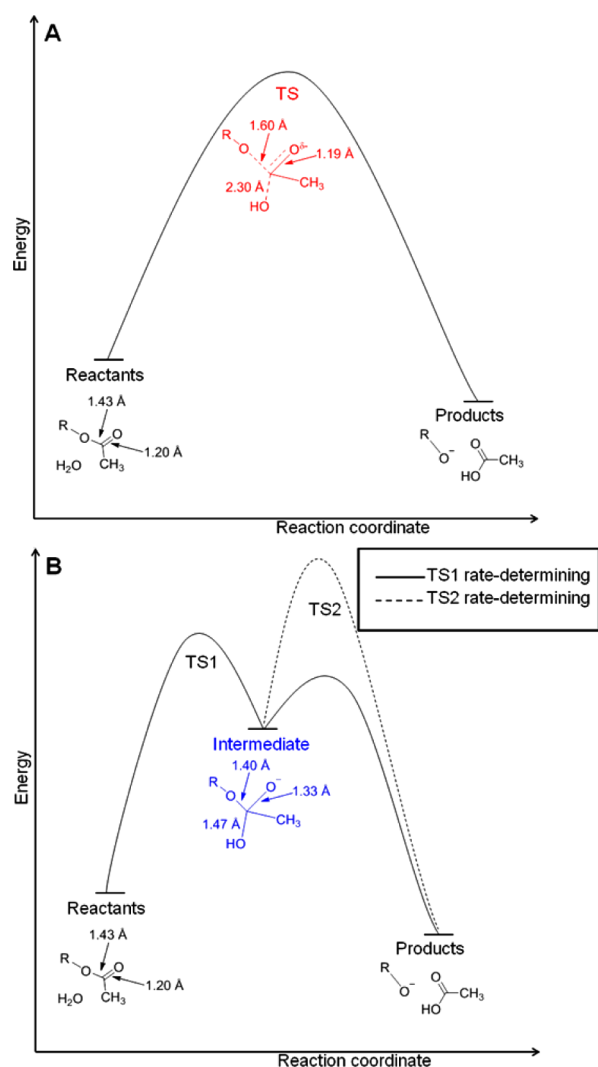
**MacroD1 Elements in TS Structure.** Transition state analysis to match the intrinsic KIEs required an Asn<sup>174</sup> mimic or second water molecule to be included in the QM calculations. These interactions mediate a shift of electron density at the carbonyl oxygen at the TS (Figure 3). The natural negative charge on the carboxyl oxygen increased from

−0.598 to −0.630 between the reactant and the TS. The main function of Asn<sup>174</sup> is to coordinate the water molecule for attack on the acetyl C-1 and to stabilize the TS. Catalytic roles for Asp<sup>184</sup> and Asn<sup>174</sup> have been previously reported in mutational studies where a 93% loss of activity in OAADPr hydrolysis occurs with alanine at these positions.<sup>1</sup>

**Electrostatic Potential Map.** Wave function analysis provides an electrostatic potential surface (ESPS) map for the TS of MacroD1 (Figure 3). The ESPS map also provides information for the design of TS analogues. This information has been useful for inhibitor design in other systems.<sup>43</sup> A MacroD1 inhibitor would be useful for dissecting the biological functions of OAADPr and related proteins. MacroD1 and related macrodomains also hydrolyze mono-ADP-riboseylated (MARylated) proteins. These include the automodified mono-ADP-riboseyltransferase ARTD10 and glycogen synthase kinase 3β (GSK3β).<sup>18,22</sup> Here, we selected OAADPr as the substrate because of the accessibility of isotopically substituted reactants and because of the link to Sirtuin pathways.

**Macrodomain Mechanisms.** Mechanisms of MacroD1 ester hydrolysis are debated. Denu and co-workers proposed a mechanism in which the ester bond is broken in a nucleophilic attack assisted by Asp<sup>184</sup> and Asn<sup>174</sup> (Asp<sup>102</sup> and Asn<sup>92</sup> in MacroD2). Rosenthal and colleagues examined macrodomain mechanisms through molecular dynamics models and mutagenesis of MacroD2, altering its activity toward ADP-riboseylated-GSK3β and ARTD10. Their studies, extrapolated to MacroD1 and OAADPr, showed a drastic decrease in activity when the proposed catalytic amino acids Asp<sup>102</sup> and His<sup>106</sup> were mutated to alanine. However, the mutants retained a small fraction of the wild-type activity suggesting participation of other residues in the active site. A molecular dynamics model of enzyme activity based on a MacroD1 crystal structure (PDB 2 × 47) agreed with the concerted mechanism supported by our TS structure. This mechanism proposed Asp<sup>184</sup> as the general base to deprotonate the nucleophilic water.<sup>18</sup>

Jankevicius et al. explored the macrodomain mechanism for deMARylation of ARTD1 and ARTD10 through mutagenesis of the putative catalytic residues in both MacroD1 and MacroD2, guided by the MacroD2-ADPr crystal structure.<sup>22</sup> The residual activity of MacroD1 when Asp<sup>184</sup> and Asn<sup>174</sup> are mutated suggested participation of other groups. In a

Scheme 1. Potential MacroD1 Mechanisms for 2-O-ADPr Hydrolysis<sup>a</sup>

<sup>a</sup>(A) The concerted mechanism for MacroD1 includes groups partially bonded to the reaction center at the TS (red). Nucleophilic participation and ester bond loss are both significant. This TS provides the best match to the intrinsic KIEs. (B) A tetrahedral intermediate mechanism (blue) was considered with TS1 or TS2 as rate-limiting steps. The mechanisms in B were eliminated as the intrinsic KIEs do not match the KIEs calculated for these TS structures.

MacroD2-ADPr crystal structure (PDB 4IQY), the conformation of the distal ribose could accommodate a 1-O-ester linkage to a MARYlated protein substrate, and this 1-hydroxyl is within the van der Waals radius of a water molecule situated between two glycine-rich loops and is coordinated by the ribose  $\alpha$ -phosphate. In molecular dynamics simulations, the ADPr  $\alpha$ -phosphate was proposed as a base to deprotonate water for attack directly onto the ribose C1 atom in a substrate-assisted, catalytic mechanism. Although OAADPr exists predominately in the 2- or 3-conformation, it is possible for the acetyl group to transesterify to the C1 position.

**Tests of the C1 Mechanism.** A test of the C1-linked mechanism by MacroD2 was hydrolysis of ARTD10-MARYlated substrate in  $\text{H}^{18}\text{O}_2$ . The assay showed incorporation into ADPr; however, a control experiment of ADPr with  $\text{H}^{18}\text{O}_2$  also

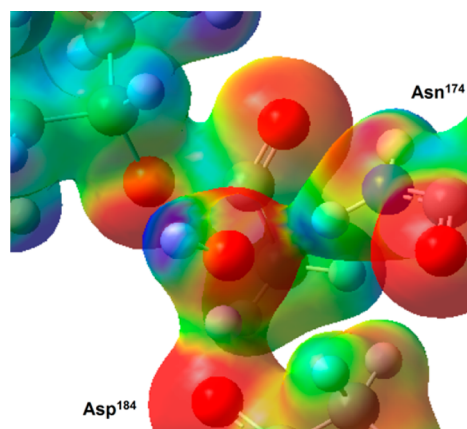


**Figure 3.** Electrostatic potential surface map of the MacroD1 transition-state. The Asp<sup>184</sup> and Asn<sup>174</sup> from MacroD1 are labeled. The map is calculated from Gaussian09 electron density and potential maps. Red indicates a relative electron enrichment, whereas blue represents an electron deficiency relative to the reactant.

showed a significant, albeit decreased, nonenzymatic incorporation. Thus, oxygen exchange at 1-O-ribose during the macrodomain catalyzed reaction is not a rigorous consequence of the proposed 1-O-hydrolysis mechanism.<sup>22</sup>

The intrinsic KIE values from OAADPr hydrolysis by MacroD1 can also be used to test the 1-hydrolysis mechanism. Transition states for the C1 hydrolysis mechanism were generated, and the KIEs calculated (SI Figure S9). The labeled atoms in the 2-ribose position are more distant from the reaction's chemical center in a C1-mechanism and give KIEs near-unity. These computational data do not support a C1 hydrolysis mechanism.

We also tested the mechanism experimentally by running the MacroD1 assay in 5% methanol. Methanol incorporation into ADPr would be expected to occur if the MacroD1 mechanism operated through a C1-ribocation, as proposed in the 1-O-ester hydrolysis mechanism. This experiment is related to the  $\text{H}^{18}\text{O}_2$  incorporation experiment, but with methanol as the alternative nucleophile. Methanol reacts with carbocations 24-fold faster than water based on the Mayr-Patz equation.<sup>44</sup> With a 20:1 ratio of water/methanol, a 1:1.2 ratio of ADPr/methoxy-ADPr would be expected as product, assuming methanol has access to the catalytic site. Mass spectrometric analysis of the reaction products detected no significant methoxy-ADPr in product or in controls lacking the MacroD1 enzyme (Figure 4). Analysis by HPLC confirmed that >50% of OAADPr was converted to products under these conditions. Thus, experimental and computational analyses make the 1-O-ester mechanism unlikely for MacroD1.

**Test of Phosphate Assistance.** Catalysis through an  $\alpha$ -phosphate substrate-assisted mechanism requires the phosphate to coordinate water. Chelation of phosphate with high  $\text{Mg}^{2+}$  ion concentration in the MacroD1 reaction would prevent the ADPr  $\alpha$ -phosphate from activating a water molecule. At a concentration of 10 mM  $\text{MgCl}_2$  and 1  $\mu\text{M}$  MacroD1, there was a 6% increase in MacroD1 activity (SI Figure S8).

Intrinsic KIEs and mechanism-based studies are consistent with a concerted 2-ester hydrolysis mechanism. However, we studied MacroD1's activity toward OAADPr, and are extrapolating some to results from MacroD1, MacroD2, and C6orf130 with MARYlated protein substrates. It is possible that

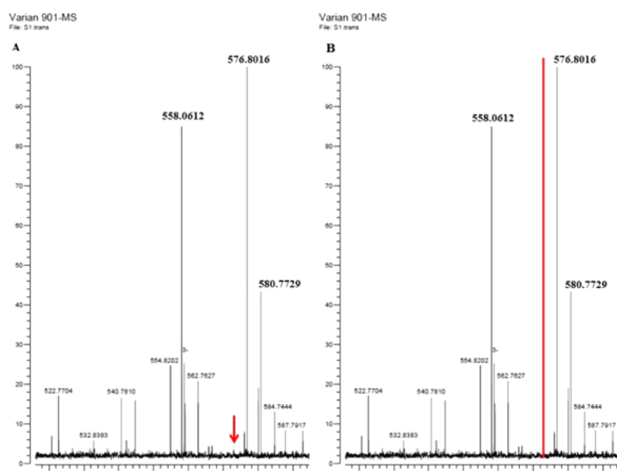


**Figure 4.** C1-methoxy-ADPribose detection. (A) The red arrow indicates where the C1-methoxy-ADPribose species would appear as a methanolysis product  $[M-H]^-$   $m/z = 572.09$ , if the mechanism proceeds through a ribocation ion mechanism. (B) Expected peak height of methoxy-ADPribose is represented in red based on observed ADPr peak response ( $m/z = 558.06$ ).

other macrodomain enzymes may operate by distinct chemical mechanisms.

**Conclusion.** Macrodomains are candidates for erasers of the mono-ADP-ribosylation of proteins and regulators of cellular OAADPr. Here, we investigate the MacroD1 TS based on intrinsic KIE values. The TS for MacroD1 catalyzed OAADPr ester hydrolysis is an early transition-state for the concerted hydrolysis of the acetyl ester by an activated water molecule. Analysis of KIEs combined with chemical experiments establish the transition state and the likely mechanism of MacroD1. Concerted ester hydrolysis catalyzed by an aspartate-activated water is the most likely mechanism of action. This mechanism may also apply to MARYlated protein substrates. The electrostatic potential map of the TS may provide information for design of analogues matching features of the TS.

## METHODS

**Materials.** 1- $^{14}\text{C}$ -Acetyl and 2- $^{3}\text{H}_3$ -acetyl acetic acid as well as 6- $^{14}\text{C}$  and 6- $^{3}\text{H}$  D-glucose were purchased from American Radiolabeled Chemicals Inc. or Moravsek Biochemicals. 2- $^{2}\text{H}$ -D-ribose, 1- $^{13}\text{C}$ -acetyl, and 2- $^{2}\text{H}_3$ -acetyl acetic acids were obtained from Cambridge Isotope Laboratories. All other reagents were purchased in the highest purity from Fisher Scientific, Sigma-Aldrich, or other industrial sources and used without further purification.

**Expression and Purification of MacroD1.** cDNA containing the sequence of human MacroD1 (BC003188.1) was obtained (Origene) and used for expression of a 6xHis-MacroD1 protein in *E. coli* as described in the Supporting Information.

**Synthesis of OAADPr.** A one-step enzymatic reaction was used to convert  $\text{NAD}^+$  into 2/3-O-AADPr. The residue Glu $^{179}$  from NAD-glycosylhydrolase of *Aplysia californica* is crucial for catalysis and the E179G mutation prevents  $\text{NAD}^+$  hydrolysis. $^{45}$   $\text{NAD}^+$  (50 mM) was added to 1 M sodium acetate at pH 5.5. Mutant E179G  $\text{NAD}^+$ -glycosylhydrolase (25  $\mu\text{M}$ ) was added to the solution and reacted overnight at 25  $^\circ\text{C}$  to quantitatively provide 1- $\alpha$ -OAADPr that rapidly and fully isomerizes to 2/3-O-AADPr. The 2/3-O-AADPr species were purified and resolved via HPLC using a 0–30% gradient of  $\text{H}_2\text{O}$  to acetonitrile (with 0.05% TFA) on a Waters Delta 600 HPLC and a Waters XSELECT CSH C18 column (5  $\mu\text{m}$ ; 4.6  $\times$  250 mm). Identity of the compounds was confirmed by mass spectrometry with an exact mass of 600.0793  $m/z$   $[M-H]$  and by  $^1\text{H}$  and  $^{13}\text{C}$  NMR that matched the previously reported compound (SI Figure S1). $^{46}$

**Synthesis of Isotopically Labeled OAADPr.** 1- $^{13}\text{C}$ -Acetyl, 1- $^{14}\text{C}$ -acetyl, 2- $^{2}\text{H}_3$ -acetyl, and 2- $^{3}\text{H}_3$ -acetyl OAADPr were synthesized from  $\text{NAD}^+$  and the corresponding acetic acid or sodium acetate with E179G  $\text{NAD}^+$ -glycosylhydrolase. All syntheses contained 1 M MES Buffer pH 5.5, 100 mM  $\text{NAD}^+$ , 10  $\mu\text{M}$   $\text{NAD}^+$ -glycosylhydrolase, and 70 mM of the labeled acetic acid or acetate. For radioactive OAADPr, 0.1–0.2 mCi of labeled acetate was used in each synthesis along with carrier.

5- $^{3}\text{H}$ , and 5- $^{14}\text{C}$  OAADPr were synthesized from commercially available isotopically labeled glucose and 2- $^{2}\text{H}$ -OAADPr from available 2- $^{2}\text{H}$  labeled ribose as described in the Supporting Information and shown in Figure S2.

2- $^{3}\text{H}$ -OAADPr was synthesized from 2- $^{3}\text{H}$ -nicotinamide mononucleotide (NMN) whose synthesis has been previously described. $^{47}$  Labeled NMN was converted to labeled  $\text{NAD}^+$  and then into 2- $^{3}\text{H}$ -OAADPr using the protocol described above.

Labeled products were purified by HPLC and lyophilized to dryness to afford a white, fluffy solid. 1- $^{13}\text{C}$ -acetyl, 2- $^{2}\text{H}_3$ -acetyl, and 2- $^{2}\text{H}$ -OAADPr were confirmed by mass spectrometry analysis (SI Figure S1), while radioactive 1- $^{14}\text{C}$ -acetyl, 2- $^{3}\text{H}_3$ -acetyl, 5- $^{3}\text{H}$ -ribose, and 5- $^{14}\text{C}$ -ribose OAADPr were confirmed by HPLC coelution with unlabeled OAADPr.

**$^{2-18}\text{O}$ -OAADPr Synthesis.**  $^{18}\text{O}$ -Uridine was synthesized as the precursor of 2- $^{18}\text{O}$ -ribose and then converted to 2- $^{18}\text{O}$ -OAADPr as described in the Supporting Information. $^{48}$  The final product was confirmed by mass spectrometry (SI Figure S1).

**Mass Spectrometry Determination of KIEs.** The kinetic isotope effects were determined using the competitive method in which isotope ratios of the OAADPr substrate were measured by mass spectrometry before and after depletion by the MacroD1 catalyzed reaction. Reactions contained 100 mM of sodium phosphate pH 6.8, 250  $\mu\text{M}$  of isotopically labeled OAADPr (heavy), 250  $\mu\text{M}$  of unlabeled OAADPr (light), and 30  $\mu\text{M}$  of MacroD1 and allowed to react at 25  $^\circ\text{C}$  for 20 min to achieve approximately 50% conversion to ADPr. OAADPr was isolated by HPLC purification, lyophilized to dryness, and stored at  $-80$   $^\circ\text{C}$ . A ThermoFisher Orbitrap Velos mass spectrometer was used to precisely determine sample isotope ratios. Samples were dissolved in 30–50  $\mu\text{L}$  of solvent (6:12:1, acetonitrile/water/acetic acid), centrifuged at 15 000 rpm for 5 min, and directly injected into the spectrometer at a rate of 4–6  $\mu\text{L min}^{-1}$ . Sample data was collected over 10 min to obtain the integrated peak area for both labeled and unlabeled OAADPr peaks. This information allowed the determination of observed KIE, as shown in eq 3, where  $f$  is the fractional conversion of product over initial substrate and  $r_0$  and  $r_1$  are the ratios of detected peak intensities for the unreacted and partially reacted samples respectively, corrected for natural isotope abundance. $^{49}$  Six individual experiments were completed for each isotopically substituted position.

$$\text{KIE}_{\text{obs}} = \frac{\ln[(1-f)(1+r_0^{-1})/(1+r_1^{-1})]}{\ln[(1-f)(1+r_0)/(1+r_1)]} \quad (3)$$

**Radiolabel Determination of KIEs.** Radioisotopically labeled OAADPrs were used to determine KIEs by the competitive method. Reactions containing 100 mM sodium phosphate at pH 6.8, 100  $\mu\text{M}$  OAADPr (a 3:1 ratio of  $^3\text{H}/^{14}\text{C}$  and at least  $5 \times 10^5$  total counts per minute, and cold carrier), and 2  $\mu\text{M}$  MacroD1 were reacted at 25  $^\circ\text{C}$  for 30 min to reach approximately 70% conversion, quenched by 1% TFA, flash frozen, and stored at  $-80$   $^\circ\text{C}$ . The remaining OAADPr was isolated by HPLC, and solvent removed under vacuum. Water (100  $\mu\text{L}$ ) and 10 mL of scintillation fluid (PerkinElmer) were added to dried samples before counting on a PerkinElmer TriCarb 2910 TR dual-channel scintillation counter. Samples were counted for 10 min and a minimum of 300 000 total counts were accumulated for each sample. Channel one contains the tritium signal, while the  $^{14}\text{C}$  signal overlaps both channels, but this overlap can be corrected based on a  $^{14}\text{C}$ -only control, as previously described. $^{50}$  Once the corrected isotope ratios of both heavy ( $^3\text{H}$  or  $^{14}\text{C}$ ) and light (either 5- $^{3}\text{H}$  or 5- $^{14}\text{C}$  remote label) channels are determined, the KIE can be solved based on eq 4 to provide the observed KIE extrapolated back to 0%

reaction.<sup>34</sup> Experiments were performed a minimum of 12 times over 4 independent experiments at each atomic position.

$$\text{KIE} = \ln(1 - f) / \ln[(1 - (fx(r_i/r_0)))] \quad (4)$$

**Computational Methods.** The TS of OAADPr ester hydrolysis was determined by Gaussian 09<sup>40</sup> quantum mechanics optimizations using density functional theory calculations with m062x in a 6-31g(d,p) basis set.<sup>41</sup> The reactant state of reactants was first determined and optimized at a global energy minimum with zero imaginary frequencies present. The transition state was determined by iterating the distances of the breaking C–O ester bond and the forming C–O nucleophile bond by 0.2 and then 0.05 Å and comparing intrinsic, experimental, and computational KIEs as determined by frequency data in ISOEFF98.<sup>42</sup> KIE values are calculated from vibrational frequency differences between both the transition and reactant states. The TS was found when sets of KIE values matched, and the resulting structure contained only one imaginary frequency for ester hydrolysis.<sup>42,51</sup>

## ■ ASSOCIATED CONTENT

### Supporting Information

This material is available free of charge via the Internet at <http://pubs.acs.org>.

## ■ AUTHOR INFORMATION

### Corresponding Author

\*Email: [vern.schramm@einstein.yu.edu](mailto:vern.schramm@einstein.yu.edu).

### Notes

The authors declare no competing financial interest.

## ■ ACKNOWLEDGMENTS

We thank the lab of R. H. Angeletti for assistance and use of their mass spectrometers, R. De Silva for the uridine phosphorylase enzyme, and the U.S. National Institutes of Health research grant GM041916 for funding.

## ■ REFERENCES

- (1) Chen, D., Vollmar, M., Rossi, M. N., Phillips, C., Kraehenbuehl, R., Slade, D., Mehrotra, P. V., von Delft, F., Crosthwaite, S. K., Gileadi, O., Denu, J. M., and Ahel, I. (2011) Identification of macrodomain proteins as novel O-acetyl-ADP-ribose deacetylases. *J. Biol. Chem.* **286**, 13261–13271.
- (2) Han, W., Li, X., and Fu, X. (2011) The macro domain protein family: Structure, functions, and their potential therapeutic implications. *Mutat. Res.* **727**, 86–103.
- (3) Karras, G. I., Kustatscher, G., Buhecha, H. R., Allen, M. D., Pugieux, C., Sait, F., Bycroft, M., and Ladurner, A. G. (2005) The macro domain is an ADP-ribose binding module. *EMBO J.* **24**, 1911–1920.
- (4) Ladurner, A. G. (2003) Inactivating chromosomes: A macro domain that minimizes transcription. *Mol. Cell* **12**, 1–3.
- (5) Neuvonen, M., and Ahola, T. (2009) Differential activities of cellular and viral macro domain proteins in binding of ADP-ribose metabolites. *J. Mol. Biol.* **385**, 212–225.
- (6) Till, S., and Ladurner, A. G. (2009) Sensing NAD metabolites through macro domains. *Front. Biosci.* **14**, 3246–3258.
- (7) Altmeyer, M., and Hottiger, M. O. (2009) Poly(ADP-ribose) polymerase 1 at the crossroad of metabolic stress and inflammation in aging. *Aging* **1**, 458–469.
- (8) Hassa, P. O., Haenni, S. S., Elser, M., and Hottiger, M. O. (2006) Nuclear ADP-ribosylation reactions in mammalian cells: Where are we today and where are we going? *Microbiol. Mol. Biol. Rev.* **70**, 789–829.
- (9) Schreiber, V., Dantzer, F., Ame, J. C., and de Murcia, G. (2006) Poly(ADP-ribose): Novel functions for an old molecule. *Nat. Rev. Mol. Cell Biol.* **7**, 517–528.

(10) Holbourn, K. P., Shone, C. C., and Acharya, K. R. (2006) A family of killer toxins. Exploring the mechanism of ADP-ribosylating toxins. *FEBS J.* **273**, 4579–4593.

(11) Messner, S., Altmeyer, M., Zhao, H., Pozivil, A., Roschitzki, B., Gehrig, P., Rutishauser, D., Huang, D., Cafilisch, A., and Hottiger, M. O. (2010) PARP1 ADP-ribosylates lysine residues of the core histone tails. *Nucleic Acids Res.* **38**, 6350–6362.

(12) Tao, Z., Gao, P., and Liu, H. W. (2009) Identification of the ADP-ribosylation sites in the PARP-1 automodification domain: Analysis and implications. *J. Am. Chem. Soc.* **131**, 14258–14260.

(13) Oberdoerffer, P., Michan, S., McVay, M., Mostoslavsky, R., Vann, J., Park, S. K., Hartlerode, A., Stegmuller, J., Hafner, A., Loerch, P., Wright, S. M., Mills, K. D., Bonni, A., Yankner, B. A., Scully, R., Prolla, T. A., Alt, F. W., and Sinclair, D. A. (2008) SIRT1 redistribution on chromatin promotes genomic stability but alters gene expression during aging. *Cell* **135**, 907–918.

(14) Scarpa, E. S., Fabrizio, G., and Di Girolamo, M. (2013) A role of intracellular mono-ADP-ribosylation in cancer biology. *FEBS J.* **280**, 3551–3562.

(15) Hassa, P. O., and Hottiger, M. O. (2008) The diverse biological roles of mammalian PARPs, a small but powerful family of poly-ADP-ribose polymerases. *Front. Biosci.* **13**, 3046–3082.

(16) D'Amours, D., Desnoyers, S., D'Silva, I., and Poirier, G. G. (1999) Poly(ADP-ribosylation) reactions in the regulation of nuclear functions. *Biochem. J.* **342** (Pt2), 249–268.

(17) Di Paola, S., Micaroni, M., Di Tullio, G., Buccione, R., and Di Girolamo, M. (2012) PARP16/ARTD15 is a novel endoplasmic-reticulum-associated mono-ADP-ribosyltransferase that interacts with and modifies karyopherin-ss1. *PLoS One* **7**, e37352.

(18) Rosenthal, F., Feijs, K. L., Frugier, E., Bonalli, M., Forst, A. H., Imhof, R., Winkler, H. C., Fischer, D., Cafilisch, A., Hassa, P. O., Luscher, B., and Hottiger, M. O. (2013) Macrodomein-containing proteins are new mono-ADP-ribosylhydrolases. *Nat. Struct. Mol. Biol.* **20**, 502–507.

(19) Mueller-Dieckmann, C., Kernstock, S., Lisurek, M., von Kries, J. P., Haag, F., Weiss, M. S., and Koch-Nolte, F. (2006) The structure of human ADP-ribosylhydrolase 3 (ARH3) provides insights into the reversibility of protein ADP-ribosylation. *Proc. Natl. Acad. Sci. U.S.A.* **103**, 15026–15031.

(20) Hassler, M., Jankevicius, G., and Ladurner, A. G. (2011) PARG: A macrodomain in disguise. *Structure* **19**, 1351–1353.

(21) Feijs, K. L., Forst, A. H., Verheugd, P., and Luscher, B. (2013) Macrodomein-containing proteins: Regulating new intracellular functions of mono(ADP-ribosylation). *Nat. Rev. Mol. Cell Biol.* **14**, 443–451.

(22) Jankevicius, G., Hassler, M., Golia, B., Rybin, V., Zacharias, M., Timinszky, G., and Ladurner, A. G. (2013) A family of macrodomain proteins reverses cellular mono-ADP-ribosylation. *Nat. Struct. Mol. Biol.* **20**, 508–514.

(23) Borra, M. T., O'Neill, F. J., Jackson, M. D., Marshall, B., Verdin, E., Foltz, K. R., and Denu, J. M. (2002) Conserved enzymatic production and biological effect of O-acetyl-ADP-ribose by silent information regulator 2-like NAD<sup>+</sup>-dependent deacetylases. *J. Biol. Chem.* **277**, 12632–12641.

(24) Liou, G. G., Tanny, J. C., Kruger, R. G., Walz, T., and Moazed, D. (2005) Assembly of the SIR complex and its regulation by O-acetyl-ADP-ribose, a product of NAD-dependent histone deacetylation. *Cell* **121**, 515–527.

(25) Tong, L., and Denu, J. M. (2010) Function and metabolism of sirtuin metabolite O-acetyl-ADP-ribose. *Biochim. Biophys. Acta* **1804**, 1617–1625.

(26) Gamble, M. J. (2013) Expanding the functional repertoire of macrodomains. *Nat. Struct. Mol. Biol.* **20**, 407–408.

(27) Sharifi, R., Morra, R., Appel, C. D., Tallis, M., Chioza, B., Jankevicius, G., Simpson, M. A., Matic, I., Ozkan, E., Golia, B., Schellenberg, M. J., Weston, R., Williams, J. G., Rossi, M. N., Galehdari, H., Krahn, J., Wan, A., Trembath, R. C., Crosby, A. H., Ahel, D., Hay, R., Ladurner, A. G., Timinszky, G., Williams, R. S., and Ahel, I. (2013) Deficiency of terminal ADP-ribose protein glycohydrolase

TARG1/C6orf130 in neurodegenerative disease. *EMBO J.* 32, 1225–1237.

(28) Herzog, N., Hartkamp, J. D., Verheugd, P., Treude, F., Forst, A. H., Feijs, K. L., Lippok, B. E., Kremmer, E., Kleine, H., and Luscher, B. (2013) Caspase-dependent cleavage of the mono-ADP-ribosyltransferase ARTD10 interferes with its pro-apoptotic function. *FEBS J.* 280, 1330–1343.

(29) Zhao, P., Lu, Y., and Han, W. (2010) Clinicopathological significance and prognostic value of leukemia-related protein 16 expression in invasive ductal breast carcinoma. *Cancer Sci.* 101, 2262–2268.

(30) Bender, M. L. (1951) Oxygen exchange as evidence for the existence of an intermediate in ester hydrolysis. *J. Am. Chem. Soc.* 73, 1626.

(31) Sims, L. B., Fry, A., Netherton, L. T., Wilson, J. C., Reppond, K. D., and Crook, S. W. (1972) Variations of heavy-atom kinetic isotope effects in SN2 displacement reactions. *J. Am. Chem. Soc.* 94, 1364–1365.

(32) Westheimer, F. H. (1961) The magnitude of the primary kinetic isotope effect for compounds of hydrogen and deuterium. *Chem. Rev.* 61, 265–273.

(33) Schramm, V. L. (1998) Enzymatic transition states and transition state analog design. *Annu. Rev. Biochem.* 67, 693–720.

(34) Cook, P. F. (1991) *Enzyme Mechanism from Isotope Effects*; CRC Press, Boca Raton.

(35) Rose, I. A. (1980) The isotope trapping method: Desorption rates of productive E.S complexes. *Methods Enzymol.* 64, 47–59.

(36) Vogel, M. J. S. a. P. C. (1971) Relative <sup>14</sup>C–<sup>13</sup>C kinetic isotope effects. *J. Chem. Phys.* 55, 2007–2013.

(37) Gardner Swain, C., Joseph, E. C. S., Reuwer, F., Jr., Lawrence, and Schaad, J. (1958) Use of hydrogen isotope effects to identify the attacking nucleophile in the enolization of ketones catalyzed by acetic acid. *J. Am. Chem. Soc.* 80, 5885–5893.

(38) Alvan, C., and Hengge, R. A. H. (1994) Concerted or stepwise mechanisms for acyl transfer reactions of p-nitrophenyl acetate? Transition state structures from isotope effects. *J. Am. Chem. Soc.* 116, 11256–11263.

(39) Lewis, B. E. and Schramm, V. L. (2006) Enzymatic binding isotope effects and the interaction of glucose with hexokinase. *Isotope Effects in Chemistry and Biology*; pp 1019–1953, CRC Taylor & Francis, Boca Raton.

(40) Frisch, M. J. T., et al. (2009) *Gaussian 09*; Gaussian, Inc.: Wallingford, CT.

(41) Yan Zhao, D. G. T. (2007) The M06 suite of density functionals for main group thermochemistry, thermochemical kinetics, non-covalent interactions, excited states, and transition elements: Two new functionals and systematic testing of four M06-class functionals and 12 other functionals. *Theor. Chem. Acc.* 120, 215–241.

(42) Anisimov, V. P., and P, J. (1999) *J. Math. Chem.* 26, 75–86.

(43) Schramm, V. L. (2013) Transition states, analogues, and drug development. *ACS Chem. Biol.* 8, 71–81.

(44) Mayr, H., and Patz, M. (1994) Scales of nucleophilicity and electrophilicity: A system for ordering polar organic and organometallic reactions. *Angew. Chem., Int. Ed. (Engl.)* 33, 938–957.

(45) Pradas, G. S., Levitt, D. G., Lee, H. C., and Stout, C. D. (1996) Crystallization of ADP-ribosyl cyclase from *Aplysia californica*. *Proteins* 24, 138–140.

(46) Szczepankiewicz, B. G., Koppetsch, K. J., and Perni, R. B. (2011) One-step, nonenzymatic synthesis of O-acetyl-ADP-ribose and analogues from NAD and carboxylates. *J. Org. Chem.* 76, 6465–6474.

(47) Burgos, E. S., Veticatt, M. J., and Schramm, V. L. (2013) Recycling nicotinamide. The transition-state structure of human nicotinamide phosphoribosyltransferase. *J. Am. Chem. Soc.* 135, 3485–3493.

(48) Dai, Q., Frederiksen, J. K., Anderson, V. E., Harris, M. E., and Piccirilli, J. A. (2008) Efficient synthesis of [2'-<sup>18</sup>O]uridine and its incorporation into oligonucleotides: A new tool for mechanistic study of nucleotidyl transfer reactions by isotope effect analysis. *J. Org. Chem.* 73, 309–311.

(49) Berti, P. J., Blanke, S. R., and Schramm, V. L. (1997) Transition state structure for the hydrolysis of NAD catalyzed by diphtheria toxin. *J. Am. Chem. Soc.* 119, 12079–12088.

(50) Silva, R. G., Veticatt, M. J., Merino, E. F., Cassera, M. B., and Schramm, V. L. (2011) Transition-state analysis of *Trypanosoma cruzi* uridine phosphorylase-catalyzed arsenolysis of uridine. *J. Am. Chem. Soc.* 133, 9923–9931.

(51) Hirschi, J. S., Takeya, T., Hang, C., and Singleton, D. A. (2009) Transition-state geometry measurements from (<sup>13</sup>C) isotope effects. The experimental transition state for the epoxidation of alkenes with oxaziridines. *J. Am. Chem. Soc.* 131, 2397–2403.